RESEARCH ARTICLE

Directionally enhanced thermoelectric effect caused by structural dislocations for in-plane heterostructures

Yuan Shang[1], Qingzhang You[2], Yuqiang Wu[1], Mengtao Sun[1,†]

[1] School of Mathematics and Physics, Beijing Advanced Innovation Center for Materials Genome Engineering, University of Science and Technology Beijing, Beijing 100083, China
[2] School of Science, Inner Mongolia University of Science and Technology, Baotou 014010, China
Corresponding author. E-mail: [†]mengtaosun@ustb.edu.cn
Received January 21, 2026; accepted March 16, 2026

Supporting Information

Supplementary Text

Section S1. The classic equations

When the free electron Fermi gas in the metal is distributed within the Fermi sphere, the free electron has a definite momentum

$$p = m_e v = \hbar k \tag{1}$$

when an electron is subjected to an electric field force, it is known by Newton's second law

$$-eE = m_e \frac{dv}{dt} = \hbar \frac{dk}{dt} \tag{2}$$

meanwhile, when considering collisions between electrons, the relaxation time (τ) is introduced, then the total current density can be expressed as

$$J = -ne(\delta v) = \frac{ne^2\tau}{m_e} E \tag{3}$$

and the conductivity is

$$\sigma = \frac{ne^2\tau}{m_e} \tag{4}$$

The Seebeck coefficient is determined by Mott equation[1]

$$S = \frac{\pi^2}{3e} k_B^2 T \frac{\partial \ln[\sigma(E)]}{\partial E}|_{E=E_F} \tag{5}$$

The electron thermal conductivity is defined as[2]

$$\kappa_e = L\sigma T \tag{6}$$

The lattice thermal conductivity is defined as[3]

$$\kappa_l = \frac{1}{3} c_v v^2 \tau \tag{7}$$

Therefore, the core of the classical equation to obtain the thermoelectric properties of materials is to obtain the electrical conductivity and relaxation time of materials, and they are only related to the intrinsic properties of materials. At the same time, the form of scalar conductivity is not suitable for anisotropic thermoelectric materials.

Section S2. Quantum transport properties

When the material scale reaches the nanometer level, the intrinsic polaron of the material will exhibit pronounced quantum effects, this can significantly affect transport characteristics.[4,5] The quantum transport theory primary objective to ascertain distribution function. The transport properties is the electric current which is evaluated using the Landauer formula[6]

$$I = \frac{2e}{h}\int T_e(E)\big(f_L(E) - f_R(E)\big)dE \tag{8}$$

where $F_e(E,\mu) = 1/e^{[(E-\mu)/k_BT}$ is the standard Fermi Dirac distribution function. $T_e(E)$ is the transmission probability and it is calculated by the standard nonequilibrium Green's function (NEGF) method. $T_e(E)$ can be calculated as[7]

$$T_e(E) = Tr(G_e^r \Gamma_L G_e^a \Gamma_R) \tag{9}$$
$$\Gamma_L = i(\sum_L^r - \sum_L^a) \tag{10}$$
$$\Gamma_R = i(\sum_R^r - \sum_R^a) \tag{11}$$
$$G_e^r = [ES - H - \sum_L^r - \sum_R^r]^{-1} \tag{12}$$

here, G_e^r is the retarded Green's function, H and S are the hamiltonian and overlap matrix, $\sum_L^r$ and $\sum_R^r$ are self-energy from left and right semi-infinite leads, respectively. Therefore, we can obtain the parameters of thermoelectric[8]

$$S = -\frac{L_1}{eTL_0} \tag{13}$$
$$\sigma = \frac{e^2 L_0}{l} \tag{14}$$
$$\kappa_e(T) = \frac{1}{Tl}\left(L_2 - \frac{L_1^2}{L_0}\right) \tag{15}$$

where l is the device length, and $L_m(\mu)$ is given by

$$L_m(\mu) = \frac{2}{h}\int_{-\infty}^{\infty} d\varepsilon T_e(\varepsilon)(\varepsilon - \mu)^m \left(-\frac{\partial f(\varepsilon,\mu)}{\partial \varepsilon}\right) \tag{16}$$

The phonon thermal conductivity can then be achieved by[8]

$$\kappa_p(T) = \frac{\hbar^2}{2\pi k_b T^2 l}\int_0^{\infty} d\omega \omega^2 T_p(\omega)\frac{e^{\hbar\omega/k_bT}}{(e^{\hbar\omega/k_bT} - 1)^2} \tag{17}$$

the phonon transmission $T_p(\omega)$ is calculated from the dynamic matrix D instead of the Hamiltonian matrix

$$T_p(\omega) = Tr\big(G_p^r \Gamma_L G_p^a \Gamma_R\big) \tag{18}$$
$$\Gamma_L = i(\sum_L^r - \sum_L^a) \tag{19}$$
$$\Gamma_R = i(\sum_R^r - \sum_R^a) \tag{20}$$
$$G_p^r = [\omega^2 - D - \sum_L^r - \sum_R^r]^{-1} \tag{21}$$

According to the above theory, in addition to the Fermi distribution of electrons and phonons of a material, the transmission coefficient is the key to determining thermoelectric parameters of materials. For the electron transport, the first step is to build Hamiltonian matrix[9]

$$H = \begin{pmatrix} H_L & \tau_L & 0 \\ \tau_L^* & H_C & \tau_R \\ 0 & \tau_R^* & H_R \end{pmatrix} \tag{22}$$

the total system is divided into the left electrode, the center zone and the right electrode. $H_{L/R}$ is the periodic Hamiltonian of the left and right electrodes, $\tau_{L/R}$ is the Hamiltonian of the electrode

coupling with the central region. For dynamic matrix D can be constructed from a matrix of force constants[10]

$$D = \frac{\partial^2 U}{\partial U_{i\alpha} \partial U_{j\beta}} \tag{23}$$

where U is the potential energy, $U_{i\alpha}$ is the displacement of atom i in the direction of α. In this paper, since all the calculations are based on the ballistic transport theory, various scattering terms are not taken into account. When the interface effect is caused by lattice mismatch in the central region, it will add a reflection term $\sum^r_{e/p_{R,(I)}}$ to the self-energy term, and the $G^r_{e/p}$ can be transformed

$$G^r_e = \left[ES - H - \sum^r_L - \sum^r_R - \sum^r_{e_R(I)}\right]^{-1} \tag{24}$$

$$G^r_p = \left[\omega^2 - D - \sum^r_L - \sum^r_R - \sum^r_{p_R(I)}\right]^{-1} \tag{25}$$

Therefore, the reflection of phonons and electrons at the interface has a significant impact on the related thermoelectric parameters.

Reference

1. K. Kanahashi, J. Pu, T. Takenobu, 2D Materials for Large-Area Flexible Thermoelectric Devices. *Adv. Energy Mater*. **10**, 1902842 (2020).
2. M. Jonson, G. Mahan, Mott's formula for the thermopower and the Wiedemann-Franz law. *Phys Rev B*. **21**, 4223-4229 (1980).
3. T. M. Tritt, Thermal Conductivity: Theory, Properties, and Applications (Springer-Verlag, 2005).
4. T. Rueckes, K. Kim, E. Joselevich, G. Y. Tseng, C. L. Cheung, C. M. Lieber, Carbon nanotube-based nonvolatile random access memory for molecular computing. *Science*. **289**, 94 (2000).
5. C. Joachim, J. K. Gimzewski, R. R. Shlitter, C. Chavy, Electronic Transparence of a Single C60 Molecule. *Phys Rev Lett*. **74**, 2102 (1995).
6. T. Jeremy, G. Hong, W. Jian, Ab initio modeling of quantum transport properties of molecular electronic devices. *Phys Rev B*. **63**, 245407 (2001).
7. T. Markussen, A. P. Jauho, M. Brandbyge, Surface decorated silicon nanowires: a route to high-ZT thermoelectrics. *Phys Rev Lett*. **103**, 055502 (2009).
8. Y. Takahiro, W. Kazuyuki, Nonequilibrium Green's function approach to phonon transport in defective carbon nanotubes. *Phys Rev Lett*. **96**, 255503 (2006).
9. Y. Meir, S. N. Wingreen, Landauer formula for the current through an interacting electron region. *Phys Rev Lett*. **68**, 2512 (1992).
10. T. Yamamoto, K. Watanabe, Empirical-potential study of phonon transport in graphitic ribbons. *Phys Rev B*. **70**, 245402 (2004).

Supplementary Figure

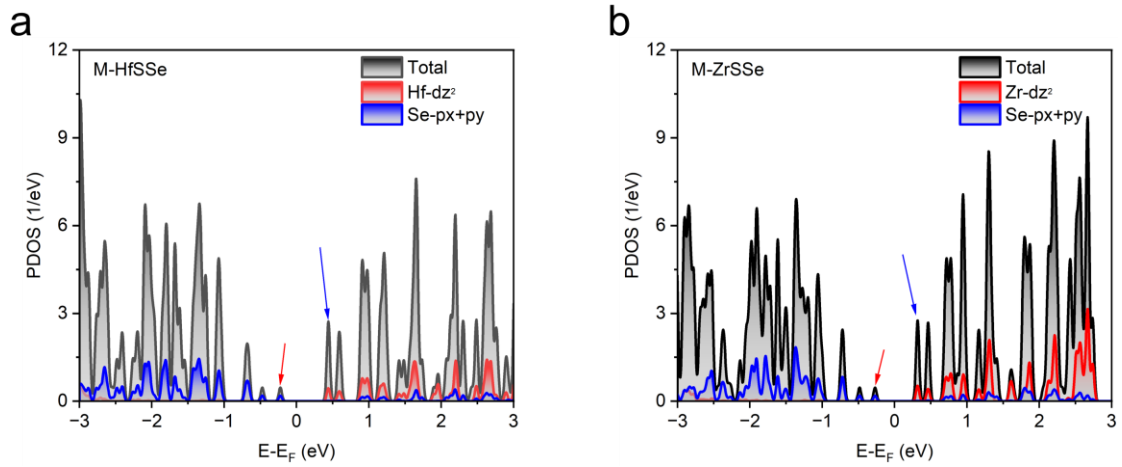

Fig. S1. Total and Projected density of state (DOS). (a) M-HfSSe (b) M-ZrSSe represent the total density of state (TDOS) and projected atomic orbital density of state (PDOS) respectively.

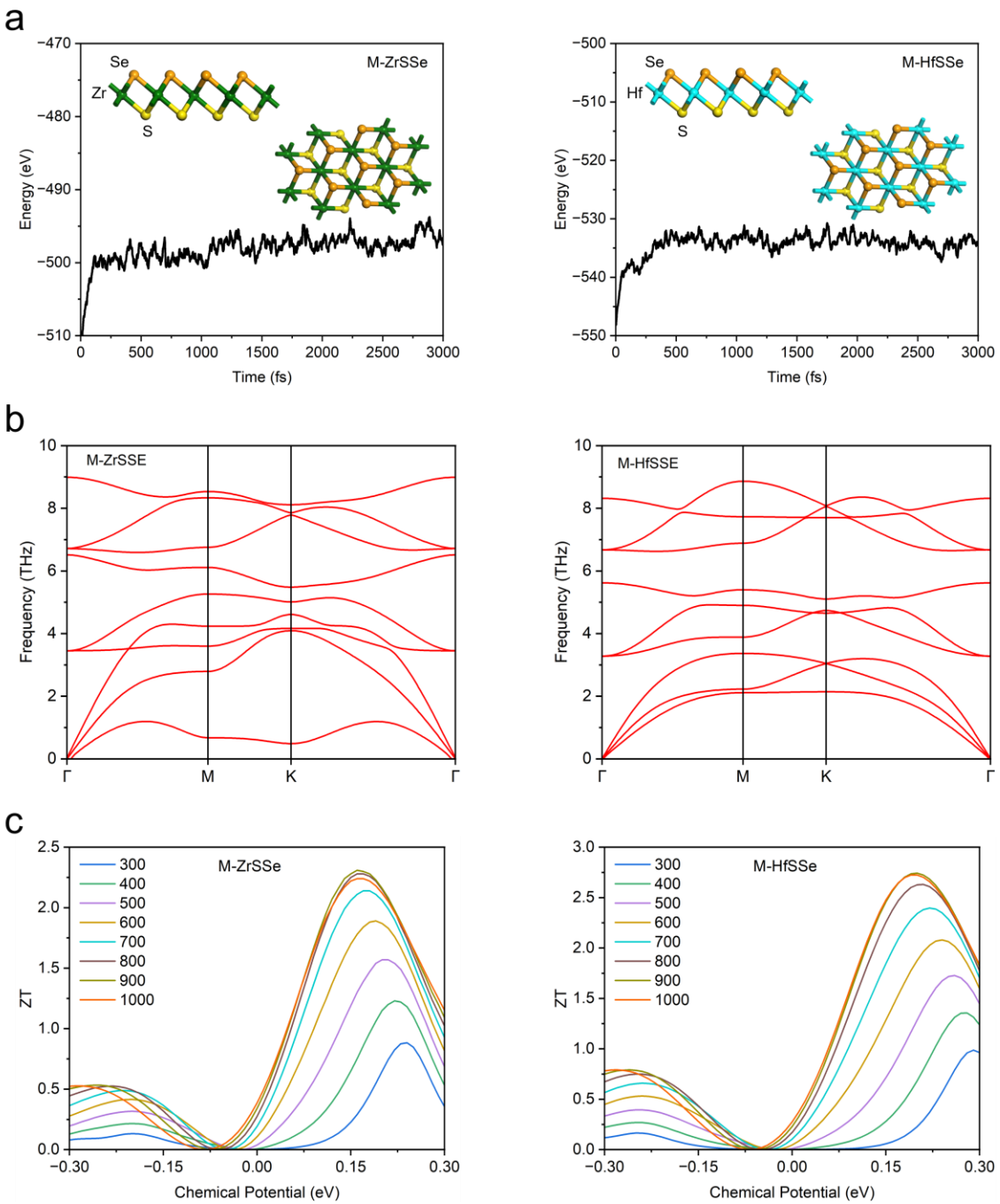

Fig. S2. Thermodynamic structure, phonon dispersion structure and ZT. The M-HfSSe and M-ZrSSe (a) thermodynamic structure energy diagram; (b) phonon dispersion spectrum; (c) function diagram of ZT with chemical formula at different temperatures.

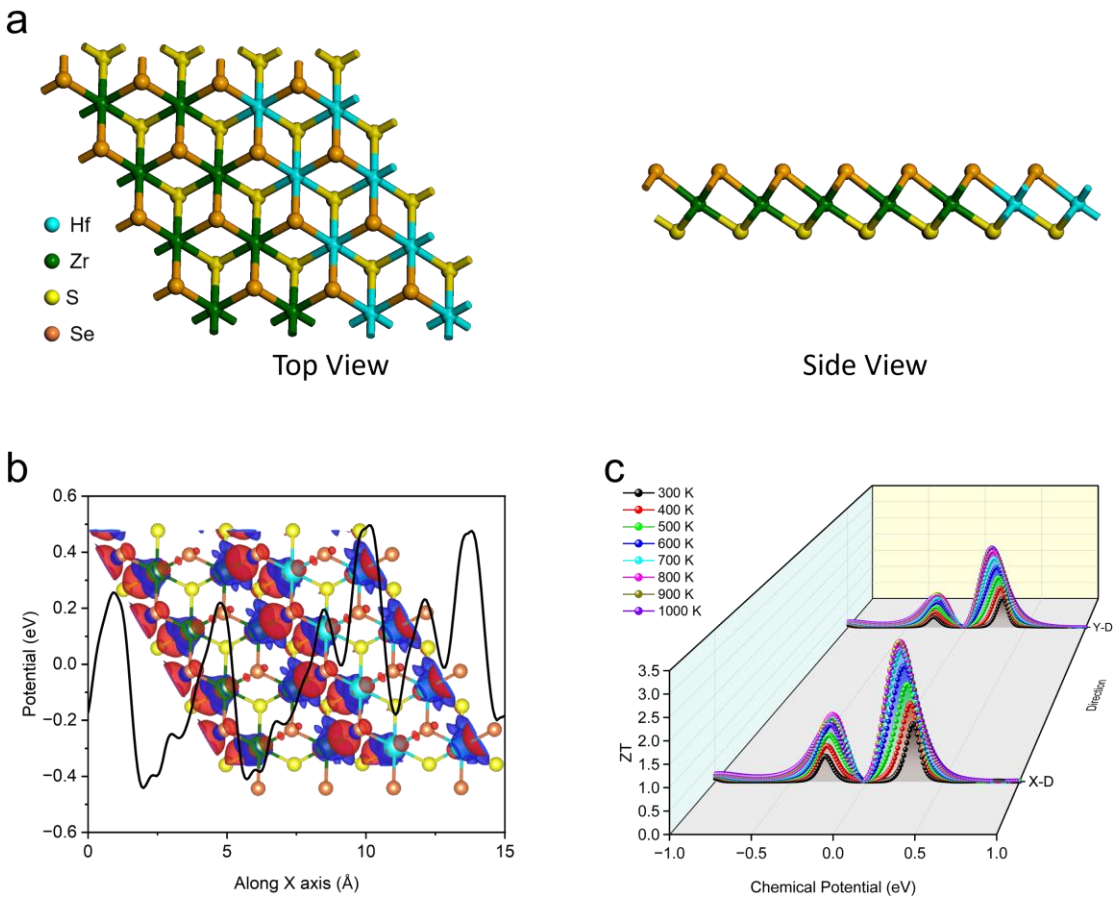

Fig. S3. Crystal structure, electronic structures and thermoelectric properties. The in-plane heterostructure constructed by two Janus monolayer materials (a) the top and side view of crystal structure; (b) the average electrostatic potential energy along the z axis and electron and charge densities (the blue (red) color represents the charge density of the electron (hole)); (c) function diagram of ZT changes with chemical potential at different temperature in two directions.

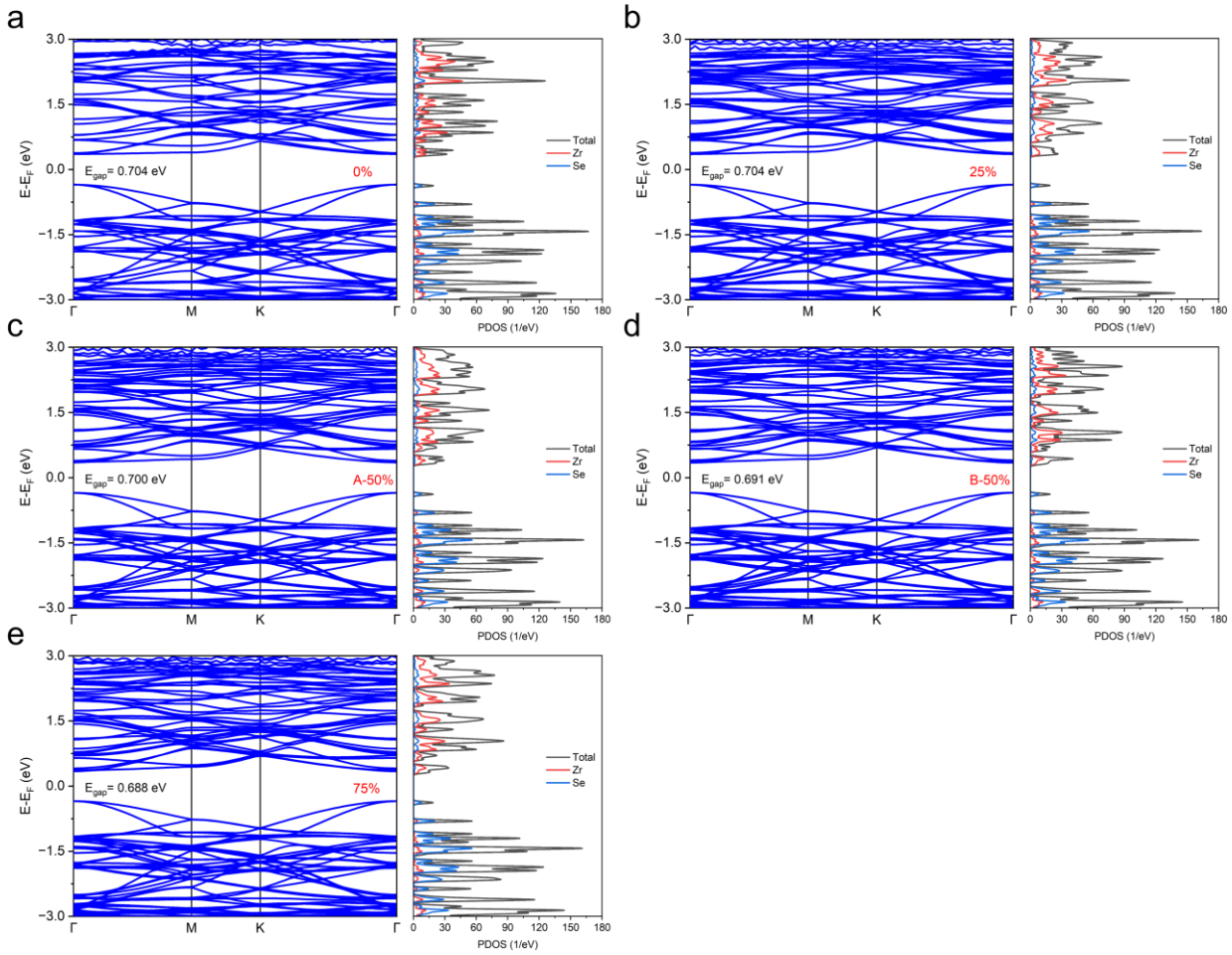

Fig. S4. Band structure and DOS. (a) $\alpha = 0\%$ (b) $\alpha = 25\%$ (c) $\alpha = A - 50\%$ (d) $\alpha = B - 50\%$ (e) $\alpha = 75\%$ is the band structure and projected atomic density of state of in-plane heterostructure, respectively.

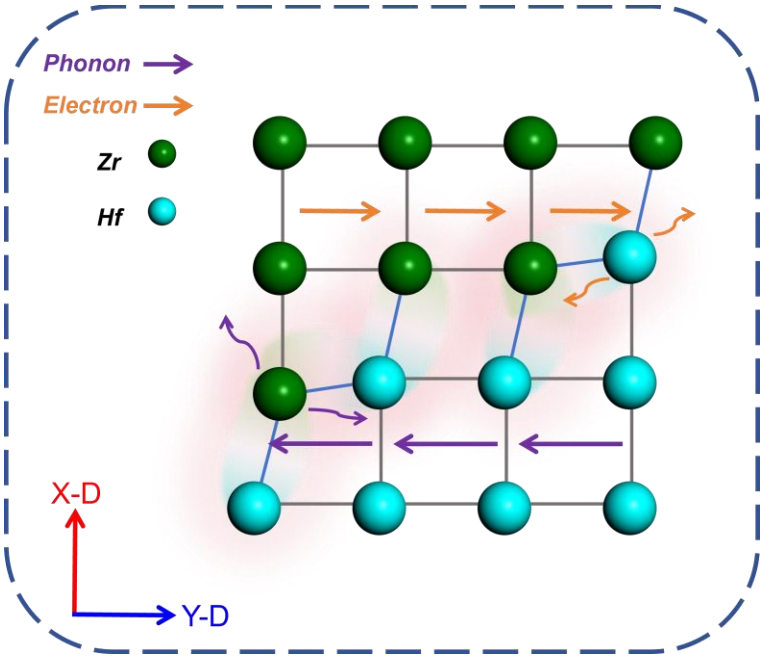

Fig. S5. motion situation of electron and phonon along the Y-D of in-plane heterostructure with structural dislocations ($\alpha = 25\%$).

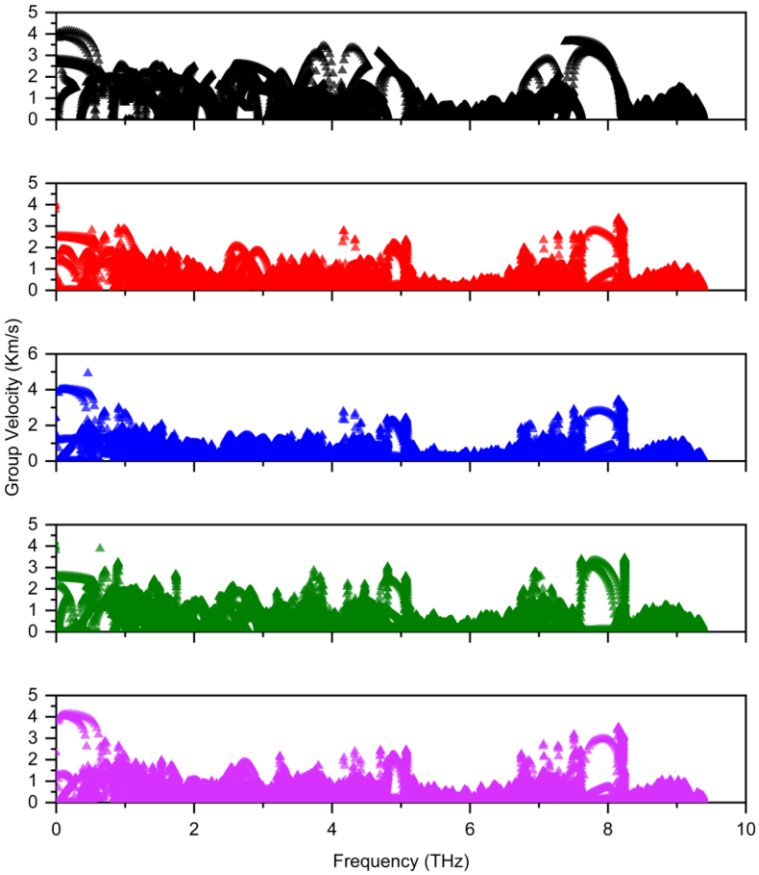

Fig. S6. The corresponding phonon group velocity of all α structure. From top to bottom, they are structures 0%, 25%, A-50%, B-50% and 75%.

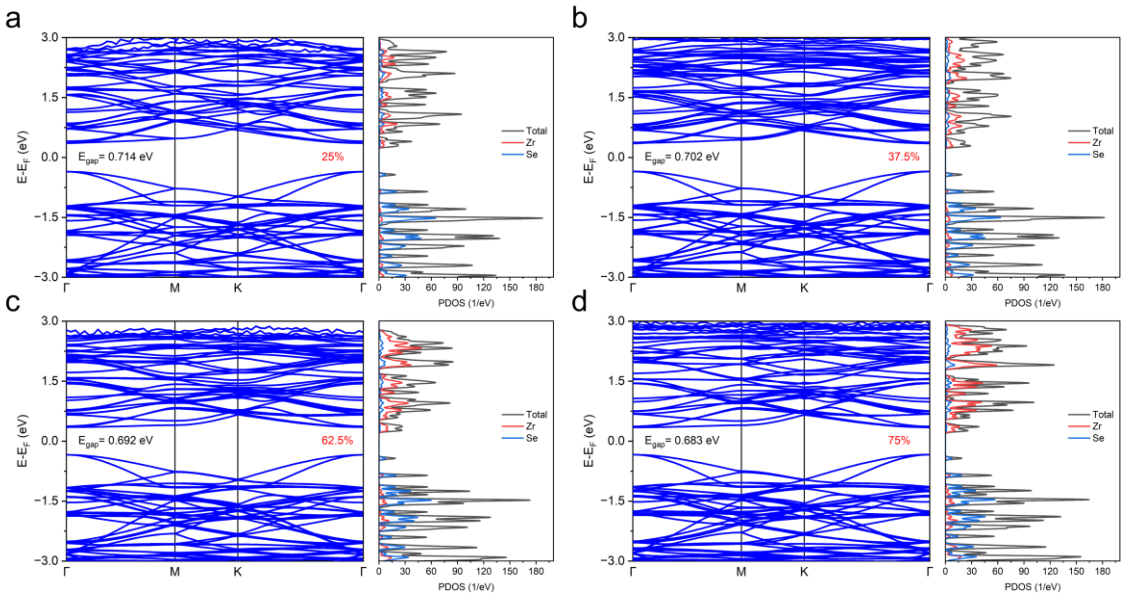

Fig. S7. Band structure and DOS. (a) $\beta = 25\%$ (b) $\beta = 37.5\%$ (c) $\beta = 62.5\%$ (d) $\beta = 75\%$ is the band structure and projected atomic density of state of in-plane heterostructure, respectively.

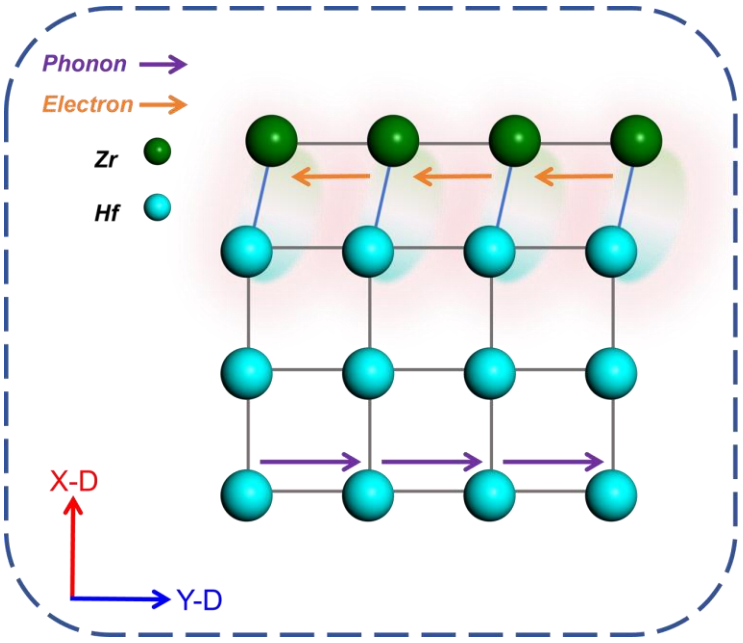

Fig. S8. Motion situation of electron and phonon along the Y-D of in-plane heterostructure with structural dislocations ($\beta = 25\%$).

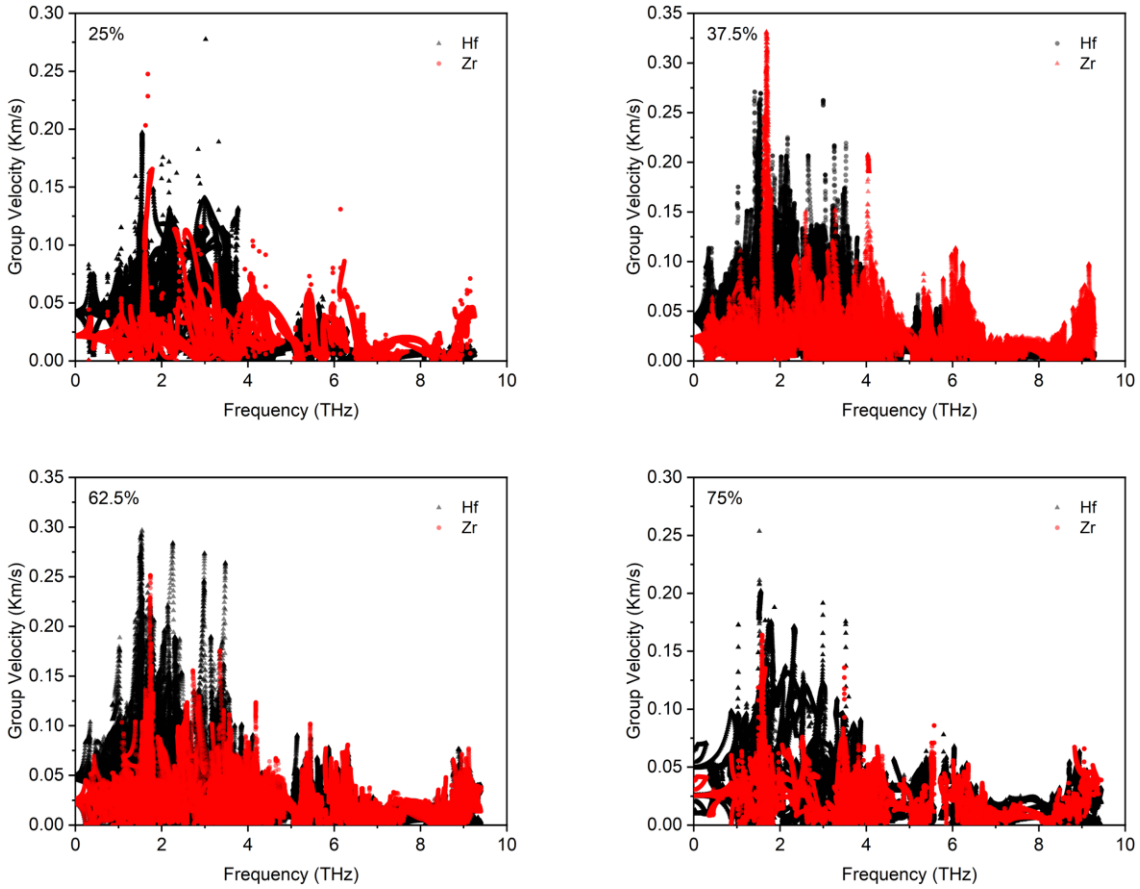

Fig. S9. Phonon state density and group velocity. The group velocity of phonon by different atoms in all β structure.

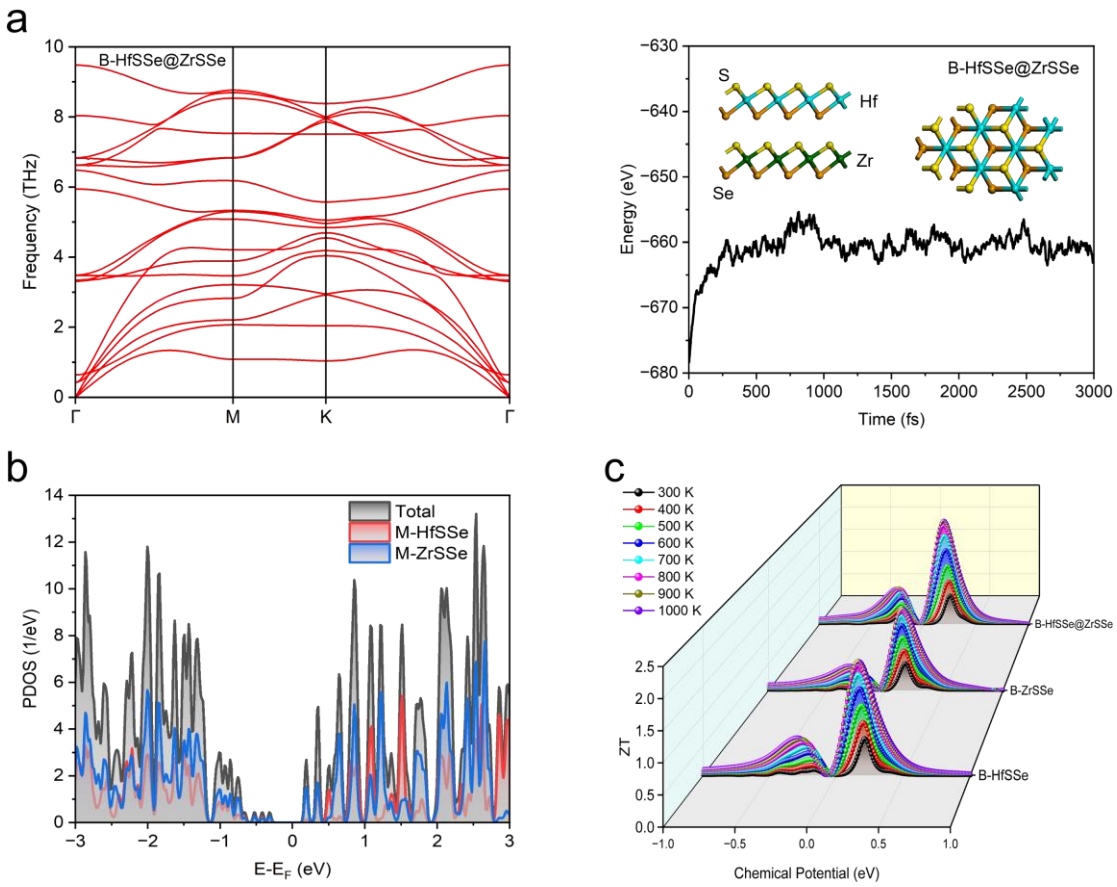

Fig. S10. Thermodynamic structure, phonon dispersion structure and ZT. The vertical heterostructure (a) phonon dispersion spectrum and thermodynamic structure energy diagram at 1000 K; (b) the total density of state (TDOS), and projected each layer density of state (PDOS). (c) Function diagram of ZT with chemical formula at different temperatures of B-HfSSe, B-ZrSSe and B-HfSSe@ZrSSe materials.

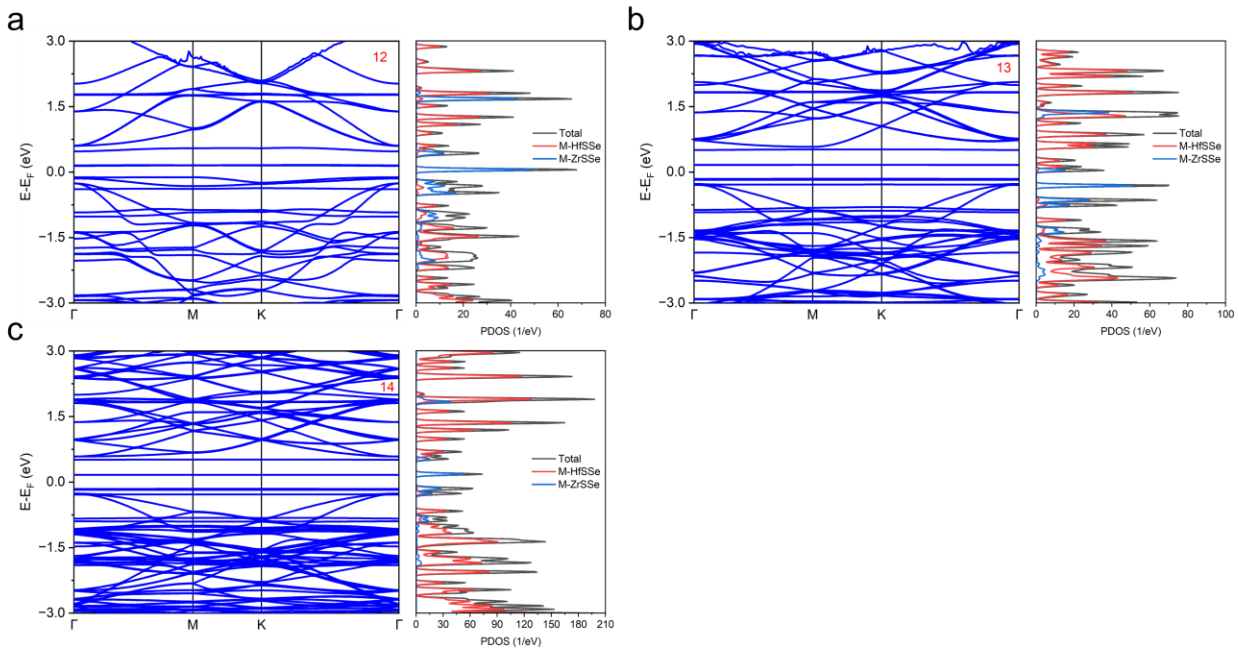

Fig. S11. Band structure and DOS. (a) 12 (b) 13 (c) 14 is the band structure and projected atomic density of state of vertical heterostructure, respectively.

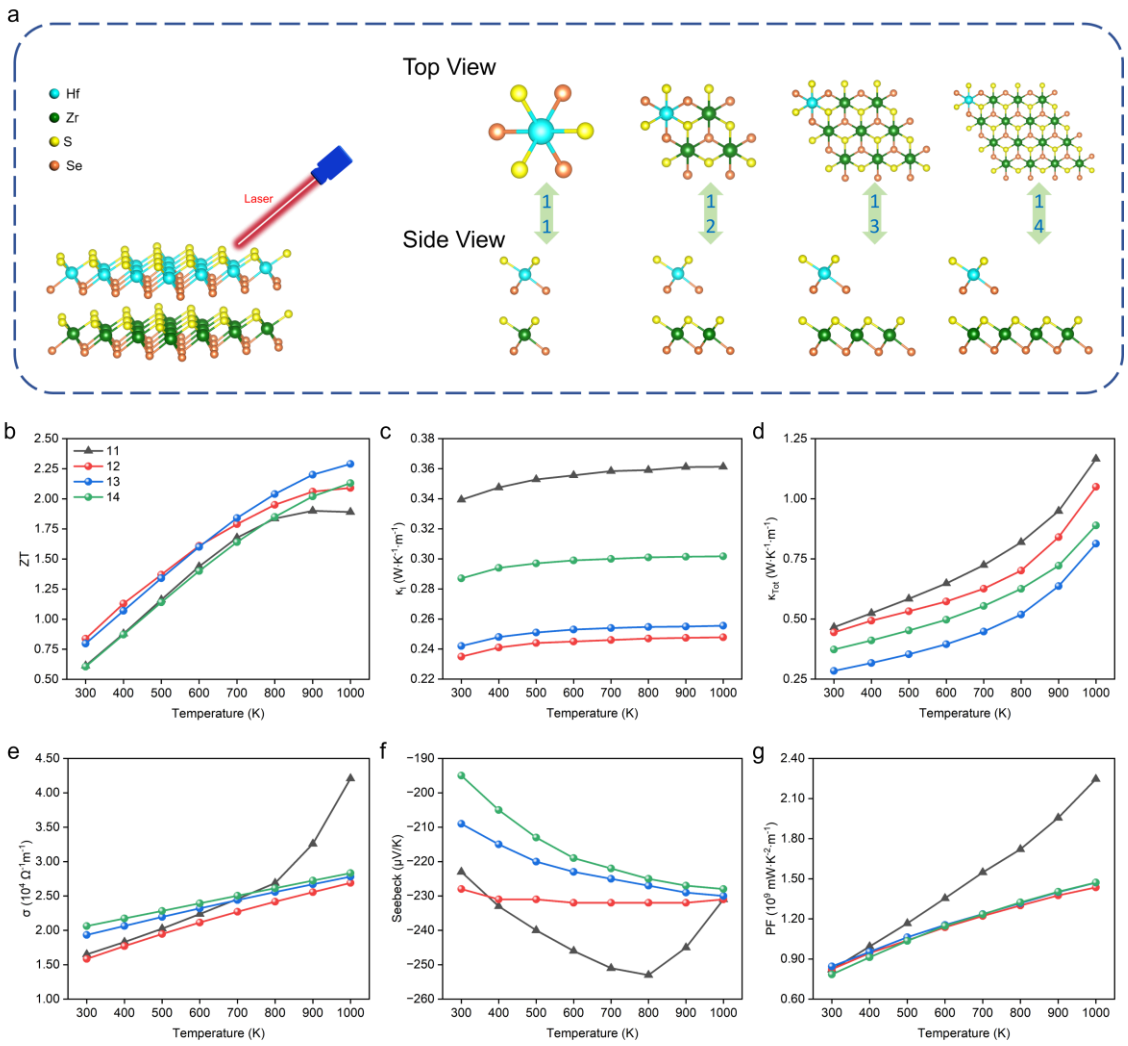

Fig. S12. Crystal structure and thermoelectric properties of the graphical superlattice vertical heterostructure. (a) Crystal structure of top and side view of a constructed graphical superlattice by laser ablation. Function diagram of (b) ZT; (c) κ_ι; (d) κ_{Tot}; (e) σ; (f) S and (g) PF with temperature for each structure.

Supplementary Table

Tabls S1: The thermoelectric ZT of various Janus monolayer structures and heterostructures.

System	Type	T (K)	ZT
M-PdSeTe[1]	N	700	2.03
	P		0.74
M-PbSSe[2]	N	300	0.81
	P		0.29
	N	900	2.99
	P		2.29
M-WSeTe[3]	P	300	0.44
	P	800	1.53
M-ZrSSe[4]	P	300	0.22
	N		1.1
M-PdSSe[5]	P	300	0.09
	N		0.07
	P	600	0.33
	N		0.26
	P	900	0.58
	N		0.49
M-PtSeTe[5]	P	300	0.91
	N		0.07
	P	600	1.97
	N		0.37
	P	900	2.54
	N		0.52
M-PtSTe[5]	P	300	0.26
	N		0.12
	P	600	0.83
	N		0.25
	P	900	1.07
	N		0.34
M-Graphene@MoSSe[6]	N	300	0.1
	N	700	0.42

Reference

1. Q. Xia, Y. S. Liu, G. Y. Gao, Enhanced thermoelectric performance andreversed anisotropy in the Janus penta-PdSeTemonolayer via biaxial strain, J. Mater. Chem. C. **13**, 5699 (2025).
2. S. L. Bai, S. B. Yang, et al. Unravelling the thermoelectric properties and suppression of bipolar effect under strain engineering for asymmetric Janus SnSSe and PbSSe monolayers, Appl Surf Sci. **599**, 153962 (2022).
3. C. Wang, Y. C. Cheng, G. Y. Gao, K. Xu, H. Z. Shao, Theoretical investigations of Janus WSeTe monolayer and related van der Waals heterostructures with promising thermoelectric performance. Appl Surf Sci. **593**, 153402 (2022).
4. S. Z. Huang, H. X. Deng, et al. Strain Tunable Thermoelectric Material: Janus ZrSSe Monolayer, Langmuir, **39**, 2728 (2023).
5. W. L. Tao, J. Q. Lan, C. E. Hu,Y. Cheng, J. Zhu, H. Y. Geng, Thermoelectric properties of Janus MXY(M = Pd, Pt; X, Y = S, Se, Te) transition-metaldichalcogenide monolayers from first principles, J. Appl. Phys. **127**, 035101 (2020).
6. N. Kumar, P. K. Sachdeva, R. Gupta, C. Bera, Theoretical Design of Highly Efficient 2D Thermoelectric DeviceBased on Janus MoSSe and Graphene Heterostructure. ACS Appl. Energy Mater. **5**, 9586 (2022).